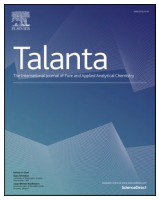
Talanta 292 (2025) 127981



Contents lists available at ScienceDirect

Talanta

journal homepage: www.elsevier.com/locate/talanta



Protein-inorganic hybrid flowers with a two-stage accelerated strategy for stimulated activation of CRISPR/Cas12a enhance polynucleotide kinase biosensing

Qi Wang [1], Xiumei Chen [1], Yang Li, Shuo Yang, Suhua Fan, Juan Xia *, Hai Wu **

Anhui Provincial Key Laboratory of Green Carbon Chemistry, Anhui Province Key Laboratory of Pollution Damage and Biological Control for Huaihe River Basin, Anhui Engineering Research Center for Functional Fruit Drink and Ecological Fermentation, School of Chemistry and Materials Engineering, Fuyang Normal University, Fuyang, Anhui, 236037, PR China

ARTICLE INFO

Keywords:
Polynucleotide kinase
Protein-inorganic hybrid flower
Terminal deoxynucleotidyl transferase
CRISPR/Cas12a
Biomarker detection

ABSTRACT

Polynucleotide kinases (PNK) play a crucial role in DNA damage repair and are closely associated with specific diseases, making them promising targets for therapeutic intervention. In this study, we propose a two-stage accelerated strategy that utilizes protein-inorganic hybrid flowers (PHFs) to enhance the performance of the terminal deoxynucleotidyl transferase (TdT)-combined CRISPR/Cas12a system (TCS) for efficient detection of PNK activity. In TCS, the participation of PHFs confines the substrate probes (SPs) to a limited space, thereby significantly enhancing the local concentration of phosphorylated 3′ termini of SPs and effectively promoting the enzymatic reaction kinetics as the first step in the accelerated strategy. Upon encountering the target PNK, the phosphorylated 3′ termini were promptly recognized and dephosphorylated to 3'−OH termini. Subsequently, TdT catalyzed the assembly of deoxyadenosine triphosphates (dATPs) without a template, rapidly activating the CRISPR/Cas12a system by forming multiple polyadenine (poly-A) chains. PHF-fixed poly-A chains then substantially boosted the localized concentration of CRISPR/Cas12a systems and vastly enhanced their efficacy in cleaving reporter nucleic acids. Our findings indicated that the spatial confinement effect facilitated by PHFs promoted frequent molecular collisions and accelerated multiple enzymatic reactions. The developed sensing strategy allows for the detection of PNK activity within a linear range of 0.001–1 U/mL, with a detection limit of 1.82×10^{-4} U/mL. Additionally, this strategy has been successfully applied to detect PNK activity in cell extracts and to screen for PNK inhibitors. Owing to these advantages, PNK can be rapidly and accurately detected with a high sensitivity, specificity, and biostability.

1. Introduction

Polynucleotide kinase (PNK), a prominent member of the 5′-kinase family, was discovered in 1965 as a bifunctional DNA end-processing enzyme with 5′-kinase and 3′-phosphatase activities [1]. It phosphorylates nucleic acid molecules at their 5′ terminus by transferring ATP γ-site phosphate groups to the 5′ hydroxyl (OH) group of single- or double-stranded DNA, RNA, oligonucleotides, or single nucleotides with 3′ phosphate groups [2]. Importantly, it can catalyze the dephosphorylation of phosphorylated polynucleotides at their 3′-terminus. Maintaining the normal activity of PNK is crucial for both the restoration of 5′-phosphate-dependent DNA and the preservation of genetic integrity. Intracellular PNK kinase activity results in atypical levels of nucleic acid phosphorylation, which is strongly associated with specific diseases, such as spinocerebellar ataxia [3], Werner syndrome [4], and neurodegenerative diseases [5]. Therefore, the accurate detection of PNK activity through the development of novel strategies is of significant practical importance for precise disease diagnosis.

Traditional PNK assay methods are limited by the radiological hazards associated with antibodies and their complexity, high cost, and poor stability [6,7]. Recently, the RNA-guided clustered regularly interspaced short palindromic repeats/CRISPR-associated nucleases (CRISPR/Cas) system rapidly evolved, known for its gene editing capabilities [8], it has been widely used for analyzing biomarkers

* Corresponding author.
** Corresponding author.
E-mail addresses: xiajuan@ustc.edu.cn (J. Xia), wuhai317@126.com (H. Wu).
[1] These authors contribute equally to this work.

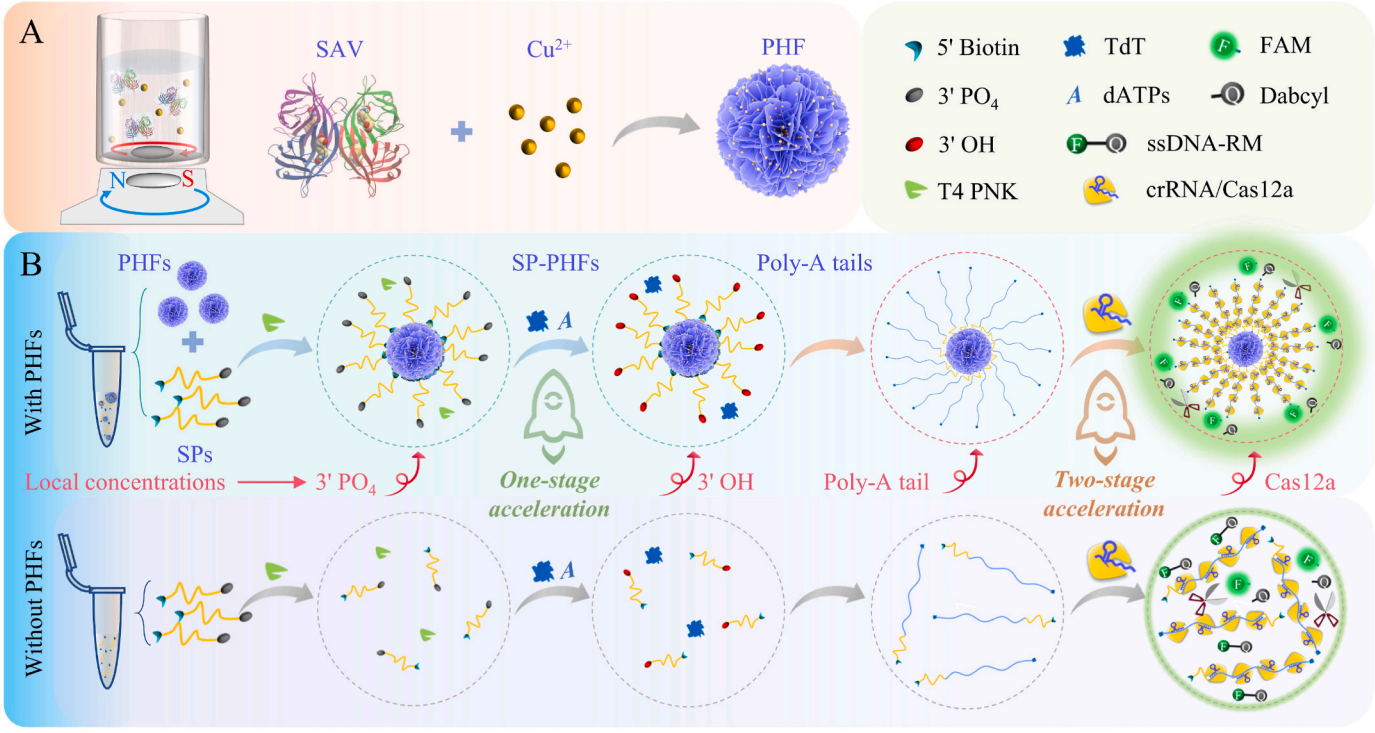
https://doi.org/10.1016/j.talanta.2025.127981
Received 12 February 2025; Received in revised form 11 March 2025; Accepted 18 March 2025
Available online 21 March 2025
0039-9140/© 2025 Elsevier B.V. All rights are reserved, including those for text and data mining, AI training, and similar technologies.

including nucleic acid [9–11], protein [12], pathogenic bacteria [13], and other targets [14]. The type 2 V-A CRISPR-associated enzyme CRISPR/Cas12a can be activated and randomly cleave single-stranded DNA reporter molecules (ssDNA-RMs) *in vitro*, in the presence of both CRISPR RNA (crRNA) and DNA targets, resulting in an amplified fluorescent signal for target detection [15,16]. In particular, when combined with nucleic acid isothermal amplification, it effectively integrates signal transduction and amplification, greatly enhancing the application of CRISPR/Cas12a in molecular diagnostics and showcasing its exceptional performance [17]. Therefore, sensing platforms using CRISPR/Cas12a systems are ideal candidates for designing and developing PNK-sensitive detection strategies.

Terminal deoxynucleotidyl transferase (TdT) catalyzes the template-independent stepwise addition of nucleotides onto an oligonucleotide chain with a 3'−OH terminus [18]. PNK facilitates the 3'−OH dephosphorylation in polynucleotide phosphorylation, thereby creating prerequisites for the functional implementation of TdT. Therefore, TdT plays a crucial role in bridging the gap between signal recognition and PNK signal transduction via the CRISPR/Cas12a system [19,20]. The TdT-combined CRISPR-Cas12a system (TCS) is a promising platform for efficient detection of PNK. However, some issues still need to be addressed in TCS strategies. Current strategies employing single-intensity-based detection systems may yield unstable results owing to the influence of concentration, local distribution of signal-reporting molecules, and fluctuations in the reaction system. Simultaneously, the intricate environment within the tested systems may have affected the stability of CRISPR/Cas12a. Importantly, according to the collision theory, increasing the concentration of reactants in a localized area increases molecular collisions, thereby enhancing the kinetics of the reaction [21]. However, the interaction between the activated Cas12a/crRNA system and ssDNA-RMs relies on random collisions in solution; this poses a challenge for effective collisions with signal reporter molecules, resulting in inefficient signal generation and low kinetics [22,23]. These aspects have often been overlooked in previous studies using Cas12a-mediated reactions.

Previous studies have demonstrated the effective utilization of nanomaterials and various enzymes to significantly enhance enzymatic reaction kinetics and stability [24–27]. Inspired by these findings, protein-inorganic hybrid flowers (PHFs) have been synthesized as a composite material featuring a self-assembled nanoflower structure formed through the specific condition-driven co-assembly of inorganic materials and proteins [28]. PHFs retain the functionality of inorganic materials and preserve the biological activity of proteins (enzymes) while significantly enhancing their activity and stability [29]. Consequently, this approach has garnered significant attention from researchers across various fields including enzyme purification, rapid detection, and chemical synthesis of enzyme catalysts [30]. However, current research on PHFs primarily focuses on enhancing the activity of the coating enzyme, with limited emphasis on using its properties to improve the reaction kinetics and signal stability [31]. Given their unique structure and functionality, PHFs with universal versatility should be designed concurrently with blueprints for PNK analysis.

Inspired by highly promising protein–inorganic hybrid technology, we leveraged the spatial confinement effect on PHFs to devise a signal amplification method based on the TCS strategy for the rapid, efficient, and reliable detection of PNK activity. PHFs were prepared via self-assembly of streptavidin (SAV) and copper ions (Cu^{2+}) (Scheme 1A). Substrate probes (SPs), equipped with biotin-modified 5′ termini and phosphorylated 3′ termini, were immobilized onto PHFs through biotin coupling with SAV to facilitate the assembly of SP-PHFs. Because of the spatial confinement effect of PHFs, the local concentration of the phosphorylated 3′ termini on SPs is theoretically higher than that of free SPs in a bulk solution. Therefore, dephosphorylation of the 3′ terminus phosphate group was more efficient when the target PNK reacted with SP-PHFs compared to its reaction with free SPs. Subsequently, by introducing TdT to respond with the dephosphorylated 3′ terminus derived from the components of SP-PHFs in a pool of deoxyadenosine triphosphates (dATPs), multiple long poly-adenine (poly-A) tails can be polymerized at the 3'−OH termini. We discovered that the reaction kinetics between TdT-polymerized multiple long poly-A tails and CRISPR/



Scheme 1. Design of TdT combined CRISPR-Cas12a sensing system for PNK detection. (A) Schematic illustration of the biomineralization reaction to prepare PHFs. (B) Using PHFs with a two-stage accelerated strategy to stimulate the activation of CRISPR/Cas12a enhances PNK biosensing.

Cas12a systems responsible for fluorescence signal transduction were significantly enhanced owing to a spatially confined effect. In summary, this enhancement significantly increased the local concentrations of the CRISPR/Cas12a system, resulting in the rapid and indiscriminate *trans*-cleavage of ssDNA-RM for the precise quantification of PNK activity.

2. Experimental section

2.1. Materials and reagents

T4 PNK (10 U/μL) with 10 × T4 PNK buffer (700 nM Tris-HCl pH 7.6, 100 mM $MgCl_2$, and 50 mM DTT) was purchased from Vazyme Biotech Co., Ltd. (Nanjing, China). TdT (5 U/μL) with 5 × reaction buffer (1 M potassium cacodylate, 0.125 M Tris, 0.05 % (v/v) Triton X-100, and 5 mM $CoCl_2$, pH 7.2 at 25 °C), T4 DNA ligase (5 U/μL) with 10 × T4 ligation buffer (400 mM Tris, pH 7.8, 100 mM $MgCl_2$, 100 mM DTT, and 10 mM ATP), Taq DNA polymerase (5 U/μL) with 10 × PCR buffer (100 mM Tris-HCl, 500 mM KCl, 15 mM $MgCl_2$, 0.8 % (v/v) and Nonidet P40, pH 8.8 at 25 °C), and RNase inhibitor (40U/μL) were purchased from Beyotime Biological Technology Co., Ltd. (Shanghai, China). EnGen Lba Cas12a (1 μM) with 10 × NEBuffer™ 2.1 (50 mM NaCl, 10 mM Tris-HCl, 10 mM $MgCl_2$, and 100 μg/mL recombinant albumin, pH 7.9 at 25 °C) and Nt.BbvCI endonuclease (10 U/μL) with 10 × Cutsmart (200 mM Tris-acetate, 100 mM magnesium acetate, 500 mM potassium acetate, and 1 mg/mL bovine serum albumin (BSA), pH 7.9 at 25 °C) were purchased from New England Biolabs Co., Ltd (Beijing, China). SAV was obtained from Macklin Biochemical Technology Co. Ltd. (Shanghai, China). BSA, 10,000 × 4S Red Plus, and 10 × DNA loading buffer were acquired from Saiguo Biotechnology Co., Ltd. (Quanzhou, China). All oligonucleotides listed in Table S1, 100 mM dATPs, and a nucleoprotein extraction kit were acquired from Sangon Biotech Co. Ltd. (Shanghai, China).

2.2. Preparation of PHFs and SP-PHFs

Protein-inorganic hybrid flowers were prepared as previously described, with modifications [32]. First, 30 μL of 0.1 mg/mL SAV and 20 μL of 0.12 M $CuCl_2{\cdot}2H_2O$ were sequentially added to 0.5 mL of 1 × phosphate-buffered saline (PBS), followed by gentle shaking in a shaker for 12 h. The reaction mixture was then centrifuged at 12,000 rpm for 5 min. The resulting precipitate was washed three times with ultrapure water and stored at 4 °C. Before PNK analysis, SP-PHFs were prepared by combining 2 μL of PHFs (50 μg/mL) with 4 μL of SPs (2 μM) and 4 μL of H_2O, followed by incubation at 37 °C for 30 min, based on specific SAV-biotin recognition. The obtained SP-PHFs were stored at 4 °C for subsequent experiments.

2.3. Characterization of PHFs and SP-PHFs

Dynamic laser scattering and phase analysis light scattering were used to determine the particle size distribution and zeta potential of the PHFs and SP-PHFs, respectively, using a NanoKyo-Omni particle size analyzer (Brookhaven, USA). Morphological characterization of the PHFs was performed using a Sigma 500 Carl Zeiss scanning electron microscope (Oberkochen, Germany). Fourier transform infrared (FT-IR) absorption peaks of the PHFs and SP-PHFs were recorded using a Nicolet 400 FT-IR spectrometer (Madison, USA). The structure of the PHFs was confirmed using X-ray diffraction analysis and X-ray photoelectron spectroscopy using a Bruker D8 Advance X-ray photoelectron spectrometer (Bruker, USA) and an ESCALAB 250Xi X-ray photoelectron spectrometer (Thermo Fisher Scientific, Waltham, MA, USA). A 12 % native gel for polyacrylamide gel electrophoresis was prepared by combining 30 % acrylamide:bis-acrylamide, 5 × Tris-borate-EDTA (TBE) buffer, 10 % ammonium persulfate, and N,N,N′,N'-tetramethylethylenediamine at room temperature. Each well was loaded with a mixture of samples pre-mixed with 10 × DNA loading buffer and 100 × 4S Red Plus. After electrophoresis in 1 × TBE buffer using a Servicebio PW-600 electrophoresis analyzer (Wuhan, China) at a voltage of 80 V for 90 min, the final gel image was captured using a ChampGel 7000 gel imaging system (Beijing, China). The characterization of PHFs and SP-PHFs is described in detail in Fig. S1.

2.4. PNK activity detection with PHFs-based TCS sensing system

To analyze PNK activity, a 30 μL reaction system containing 10 μL of SP-PHFs, 1 μL of T4 PNK (10 U/mL), 3 μL of 10 × T4 PNK buffer, 1 μL of TdT (5 U/μL), 6 μL of 5 × reaction buffer, 2 μL of dATPs (100 mM), and 7 μL of H_2O was mixed and incubated at 37 °C for 20 min. In the CRISPR/Cas12a reaction system, 4 μL of Cas12a (1 μM), 4 μL of crRNA (1 μM), 5 μL of 10 × NEBuffer™ 2.1, and 5 μL H_2O were mixed and incubated at 25 °C for 10 min. Subsequently, a mixture of 30 μL of product containing TdT-polymerized multiple long poly-A tails, 18 μL of pre-mixed CRISPR/Cas12a reaction solution, and 2 μL of ssDNA-RM (10 μM) was incubated at 37 °C for 10 min. Subsequently, 150 μL of H_2O was introduced into the reaction mixture, resulting in a final volume of 200 μL, which was then transferred to a microcuvette for fluorescence measurement. The fluorescence spectra were measured using a PerkinElmer FL8500 fluorescence spectrophotometer (Thermo Fisher Scientific, Waltham, MA, USA) with excitation at 493 nm, emission ranging from 505 to 650 nm, slit width of 10/5 nm, scanning speed of 240 nm/min, and PMT voltage of 700 V. Real-time fluorescence was monitored to evaluate the assay performance using a Bio-Rad CFX Connect real-time PCR system (Hercules, CA, USA). It is worth noting that the concentrations in this study were calculated based on a final test volume of 200 μL.

2.5. Cell culture and T4 PNK activity analysis in cell extracts

HeLa cells (cervical cancer cells) were used to evaluate the intracellular PNK activity. All cells were cultured in T25 flasks in complete culture medium and incubated at 37 °C with 5 % CO_2 in a cell incubator (Thermo Fisher Scientific, Waltham, MA, USA). The cultured cells were rinsed with cold PBS and detached by trypsin digestion. The cell density was determined using a Countstar BioTech automated cell counter (Countstar, China). Cell extracts were obtained using a nucleoprotein extraction kit as required and subsequently stored at −80 °C for future use. The detection procedure was similar, except that T4 PNK was replaced with cell extract.

3. Results and discussion

3.1. Principle of PHFs-based two-stage accelerated strategy for T4 PNK-responsive detection

Scheme 1B illustrates a two-stage acceleration strategy utilizing PHFs to stimulate the TCS for enhanced PNK biosensing. Conversion of the target PNK signal into a readable fluorescent signal involves two distinct steps. In the initial step (Scheme 1B), the dephosphorylation of SPs' 3′-PO_4 termini catalyzed by T4 PNK resulted in the generation of 3'−OH termini. Subsequently, using TdT and dATPs, multiple long poly-A tails were extended from the 3'−OH terminus. In this process, PHFs can immobilize SPs in a confined space, significantly increasing the local concentration of the phosphorylated 3′ terminal. As a result, it enhances the effective subsequent collision between the 3′-PO_4 termini and PNK, as well as between the 3'−OH termini and TdT, leading to a substantial improvement in the enzymatic reaction kinetics, which is the first-order acceleration process.

In the second stage (Scheme 1B), the CRISPR/Cas12a system was activated using extended poly-A tails as templates in the presence of the crRNAs. The *trans*-cleaving activity of CRISPR/Cas12a was used to cleave ssDNA-RMs and randomly generate fluorescence signals. During this process, PHFs confined many poly-A products within a limited

space, leading to locally high concentrations of poly-A tails, which significantly enhanced their binding efficiency to Cas12a/crRNA. Importantly, the longer poly-A tail enabled the binding of a greater amount of Cas12a/crRNA, thereby effectively confining multiple CRISPR/Cas12a systems within a limited space. This allows for more efficient and rapid cleavage of ssDNA-RM, releasing a strong fluorescent signal that indicates the concentration of the detected target. Without PNK, TdT cannot extend the 3′-PO_4 termini on SPs, resulting in a lack of poly-A tails for activating CRISPR/Cas12a systems, leading to a low fluorescence signal. In this study, we engineered a crRNA recognition region for the poly-A tail, consisting of 23 uridine (U) nucleotides. Furthermore, we synthesized an ssDNA consisting of 30 adenine (A) bases, named poly-A^{30}. We examined the response of the CRISPR/Cas12a sensing system using poly-A^{30} as an activator. In the presence of poly-A^{30}, the gel electrophoresis and fluorescence spectra in Fig. S2 demonstrated that the complement of the crRNA with poly-A^{30} initiates the *trans*-cleavage activity of Cas12a. Based on these results, we are confident that implementing a two-stage acceleration strategy based on PHFs can effectively enhance the activity of TdT-combined CRISPR/Cas12a, enabling the efficient and stable detection of PNK.

3.2. PHFs-based TCS can be used for PNK sensing

To demonstrate the practicality of our strategy for PNK detection, we measured fluorescence intensity in the presence and absence of PNK to analyze the responsiveness of the PHF-based TdT-combined CRISPR-Cas12a system. First, we investigated the effect of T4 PNK, TdT, or both on the fluorescence intensity in the presence of SPs (Fig. 1A). The absence of either enzyme failed to trigger CRISPR-Cas12a. In the absence of T4 PNK, as depicted in Fig. 1B, dephosphorylation of the 3′ termini of the SPs was hindered. Consequently, relying solely on TdT cannot effectively activate the CRISPR-Cas12a system or accomplish the *trans*-cleavage of ssDNA-RM (lane a). Similarly, no significant increase in the fluorescence signal was observed in the absence of TdT (lane b). However, in the presence of both T4 PNK and TdT, the 3′ termini of SPs undergo dephosphorylation. Subsequently, the resulting 3’−OH termini were elongated into poly-A tails using dATPs as substrates, with the assistance of TdT. The activation process ultimately triggered the CRISPR-Cas12a system, leading to a significant increase in the signal value (lane c) by approximately 415.95 % [$(F - F_0/F_0) \times 100$ %], accompanied by a signal-to-noise (S/N, F/F_0) ratio of 5.16 (inset in Fig. 1B). F and F_0 represent the peak fluorescence signal values acquired from samples with and without T4 PNK, respectively. Therefore, the products extended by TdT after T4 PNK-activated SPs can be used to initiate the CRISPR-Cas12a system for fluorescent signal transduction, thereby demonstrating the feasibility of T4 PNK detection. Subsequently, we examined the changes in the fluorescence intensity of SP-PHFs in the presence of T4 PNK, TdT, or a combination of both (Fig. 1C). Fluorescence intensity was maintained at a low level in the presence of either T4 PNK or TdT (lanes d and e). However, it significantly increased in the presence of both enzymes (lane f), with a signal increase of approximately 826.64 % and an S/N ratio of 8.84 (Fig. 1D). This demonstrates the feasibility of using a PHF-based TCS to detect the target T4 PNK, and indirectly proves that PHFs can enhance the efficiency of fluorescence signal transduction.

3.3. PHFs-based two-stage acceleration strategy enhances TCS

The rate of the enzymatic reaction of T4, PNK, and TdT directly determines the effect of first-stage acceleration. To assess the influence of PHFs on enzymatic reactions, we synthesized ssDNA consisting of 30 thymine (T) bases (poly-T^{30}) and incorporated an inverted dT at the 3′

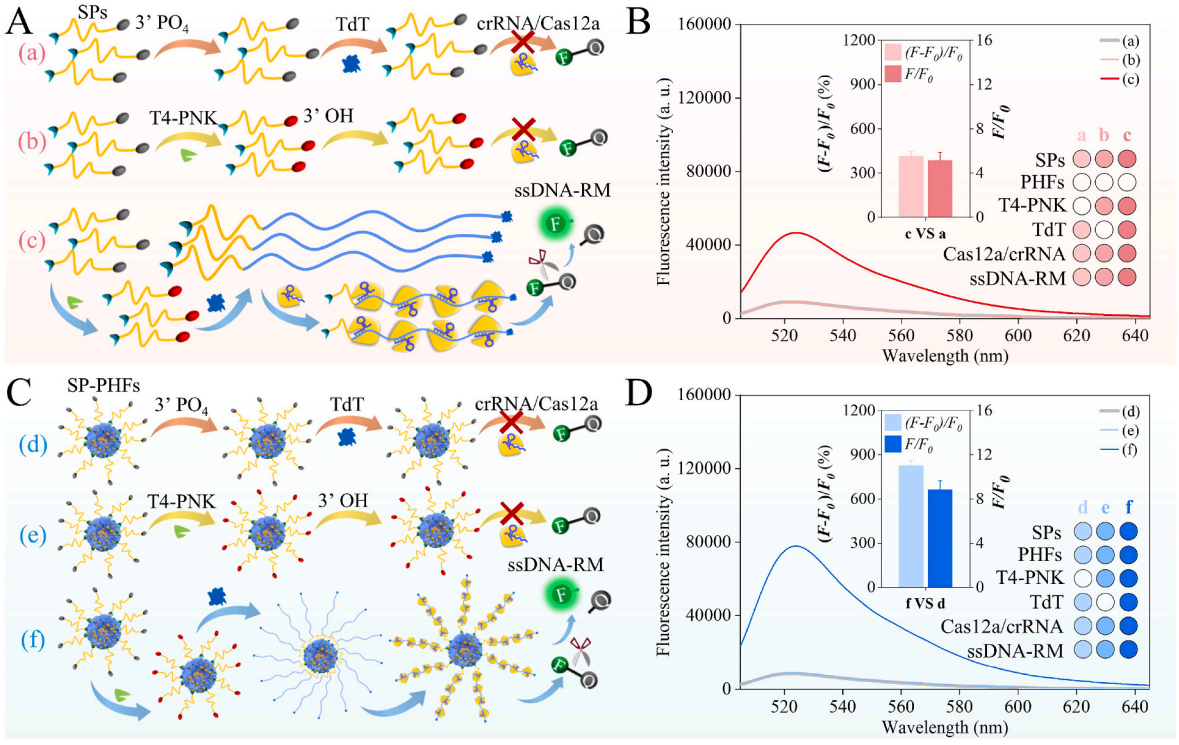


Fig. 1. Feasibility validation of PHFs-TCS system. (A) The application of SPs in detecting T4 PNK and (B) the corresponding fluorescence spectral analysis under three conditions: (a) TdT only, (b) T4 PNK only, and (c) TdT + T4 PNK. (C) The application of SP-PHFs in detecting T4 PNK and (D) the corresponding fluorescence spectral analysis under three conditions: (a) TdT only, (b) T4 PNK only, and (c) TdT + T4 PNK. The data represents the mean values obtained from three repetitive experiments, with error bars indicating the standard deviations. Experimental conditions: [PHFs] = 0.50 μg/mL, [SPs] = 40 nM, [T4 PNK] = 0.05 U/mL, [TdT] = 25 U/mL, [dATPs] = 1 mM, [Cas12a] = 20 nM, [crRNA] = 20 nM, and [ssDNA-RM] = 100 nM. The enzymatic reaction time for T4 PNK and TdT was 20 min, while the reaction time for the CRISPR/Cas12a system was 10 min.

terminus to prevent elongation by TdT [33]. Poly-A tails generated through extension can pair with poly-T^{30} sequences via complementary base pairing to form double-stranded DNA (dsDNA). Subsequently, SYBR Green I emitted a strong fluorescence signal when intercalated into dsDNA, enabling monitoring of T4 PNK and TdT enzymatic reaction rates. We examined variations in fluorescence intensity when PHFs were present or absent (Fig. 2A). As shown in Fig. 2B, in the absence of SPs, solution systems containing TdT, poly-T^{30}, and SYBR Green I exhibited low fluorescence signal maintained at a low level (lane a). Fluorescence signals were not enhanced by the addition of PHFs or T4 PNK (lanes b and c). However, even in the presence of SPs, the absence of T4 PNK failed to trigger any fluorescent signals (lanes d and f). The fluorescence signal value gradually increased over time when SPs and T4 PNK were added simultaneously (lane e), whereas the addition of PHFs resulted in more rapid and continuous enhancement of the fluorescence signal (lane g). PHF-based assays achieved significantly higher fluorescence values of 1189.52, 1565.83, and 1595.34 at 10, 30, and 60 min, respectively, compared to the assays without PHFs (fluorescence values of 673.86, 1173.01, and 1315.59 at 10, 30, and 60 min, respectively). The fluorescence intensity ratio reached 1.77 at the 10-min mark. Thus, PHFs enhanced the effective subsequent collision between the 3′-PO_4 termini and PNK and between the 3’−OH termini and TdT, leading to a substantial improvement in enzymatic reaction kinetics, the first-order acceleration process.

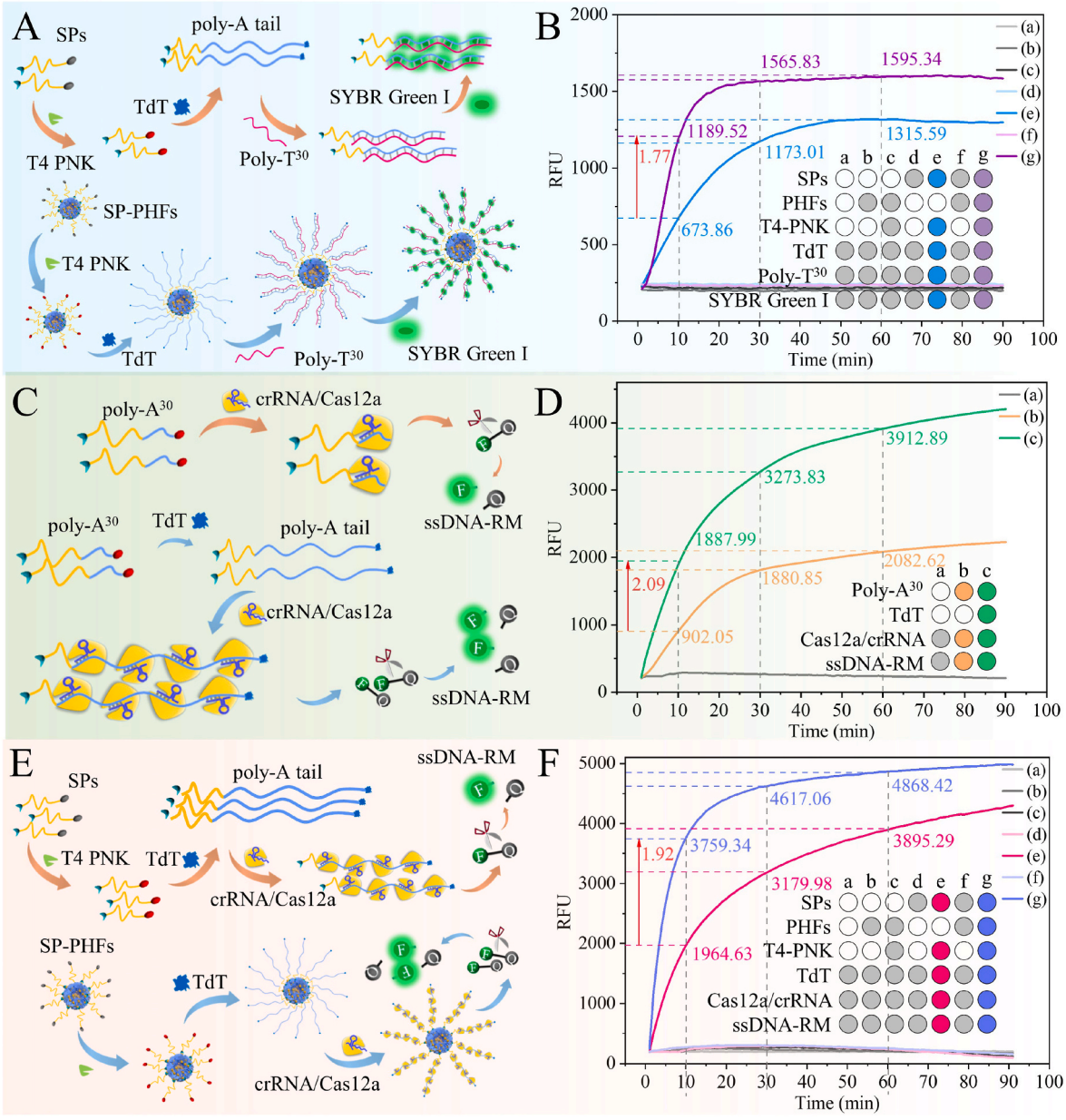


Fig. 2. Evaluation of PHFs-based two-stage acceleration strategy. (A) Evaluation of PHFs-based two-stage acceleration strategy. (B) Time-dependent fluorescent responses of PHFs, SPs, and SP-PHFs in the solution systems containing TdT, poly-T^{30}, and SYBR Green I before and after adding T4 PNK over 90 min. (C) Schematic of TdT effect on poly-A^{30}-activated Cas12a/crRNA cleavage. (D) Time-dependent fluorescent responses of poly-A^{30} in the solution systems containing Cas12a/crRNA and ssDNA-RM before and after adding TdT over 90 min. (E) Schematic of PHFs effect on Cas12a/crRNA cleavage. (F) Time-dependent fluorescent responses of PHFs, SPs, and SP-PHFs in the solution systems containing TdT, Cas12a/crRNA, and ssDNA-RM before and after adding T4 PNK over 90 min. The red arrows in Fig. 2B–D, and F indicate the fluorescence intensity ratio at 10 min, comparing conditions with and without PHF or poly-A^{30}. Experimental conditions: 0.1 × SYBR Green I, [PHFs] = 0.50 μg/mL, [SPs] = [poly-T^{30}] = [poly-A^{30}] = 40 nM, [T4 PNK] = 0.05 U/mL, [TdT] = 25 U/mL, [dATPs] = 1 mM, [Cas12a] = 20 nM, [crRNA] = 20 nM, and [ssDNA-RM] = 100 nM. (For interpretation of the references to colour in this figure legend, the reader is referred to the Web version of this article.)

The efficiency of ssDNA-RM *trans*-cleavage by CRISPR/Cas12a systems directly determines the effectiveness of second-stage acceleration. To assess the impact of varying amounts of Cas12a protein bound to poly-A tails on the efficiency of Cas12a/crRNA-mediated cleavage of ssDNA-RM (Fig. 2C), we used poly-A^{30} and TdT-extended poly-A^{30} as template DNAs to activate the CRISPR/Cas12a system. Theoretically, TdT can be equipped with 100–130 dATPs at the 3′ terminus of poly-A^{30} or even longer [34], allowing the extended poly-A^{30} to bind multiple Cas12a proteins. Each Cas12a/crRNA complex requires approximately 20–25 nt of a complementary sequence for stable binding [35]. In our system, the crRNA contained 23 U nucleotides that hybridized to the poly-A tail via A-U base pairing. Thus, for a poly-A tail of approximately 130 nt, the theoretical maximum number of bound Cas12a-crRNA complexes was approximately six. In addition, steric hindrance and overlapping binding sites reduced this number; each poly-A tail may bind to approximately five Cas12a-crRNA complexes. In contrast, untreated poly-A^{30} could only accommodate one Cas12a protein. Fig. 2D shows the minimal background fluorescence signal without poly-A^{30} (lane a). However, when the CRISPR/Cas12a system was combined with poly-A^{30}, Cas12a/crRNA was activated and effectively cleaved ssDNA-RM, releasing a detectable fluorescence signal (lane b). In contrast, extending poly-A^{30} with TdT to form a poly-A tail can increase the local concentration of Cas12a/crRNA by fixing more of it, thereby effectively enhancing the collision rate between Cas12a/crRNA and ssDNA-RM. The cleavage efficiency of Cas12a/crRNA was significantly enhanced, leading to a rapid increase in the fluorescence intensity over time (lane c). At 10 min, detection based on poly-A tails achieved a fluorescence value of 1887.99, which was significantly higher than that obtained by detection based on poly-A^{30} (902.05), resulting in a fluorescence intensity ratio of 2.09. Fixing Cas12a/crRNA-bound poly-A tails to PHFs further increased the local concentration of Cas12a/crRNA, resulting in a higher collision rate between Cas12a/crRNA and ssDNA-RM (Fig. 2E). Fig. 2F illustrates that the activation of Cas12a/crRNA for *trans*-cleaving ssDNA-RM was unsuccessful in the absence of SPs or T4 PNK (lanes a, b, c, d, and f). Fixing Cas12a/crRNA/poly-A complexes to PHFs significantly enhanced the cleavage efficiency of Cas12a/crRNA (lane g), resulting in more efficient fluorescence production than when it was not fixed to PHFs (lane e e). Even after 10 min, the PHF-based two-stage acceleration strategy achieved a fluorescence value of 3759.34, which was significantly higher than that obtained without the PHFs sensing strategy (1964.63), resulting in a fluorescence intensity ratio of 1.92. This trend suggests that PHFs provide more positive feedback with increasing reaction times. The primary advantage of PHFs is their ability to maximize the local concentration of reactants, thereby confining their reactions to a specific space. This reduces the diffusion distance and increases the likelihood of frequent collisions between reactants, thereby promoting efficient reactions. This sharp difference provides further evidence of the spatial confinement effect when PHFs are used as a scaffold to enhance the detection of PNK activity. These results demonstrate the exceptional efficacy of a two-stage acceleration strategy based on PHFs for the ultrasensitive detection of PNK activity.

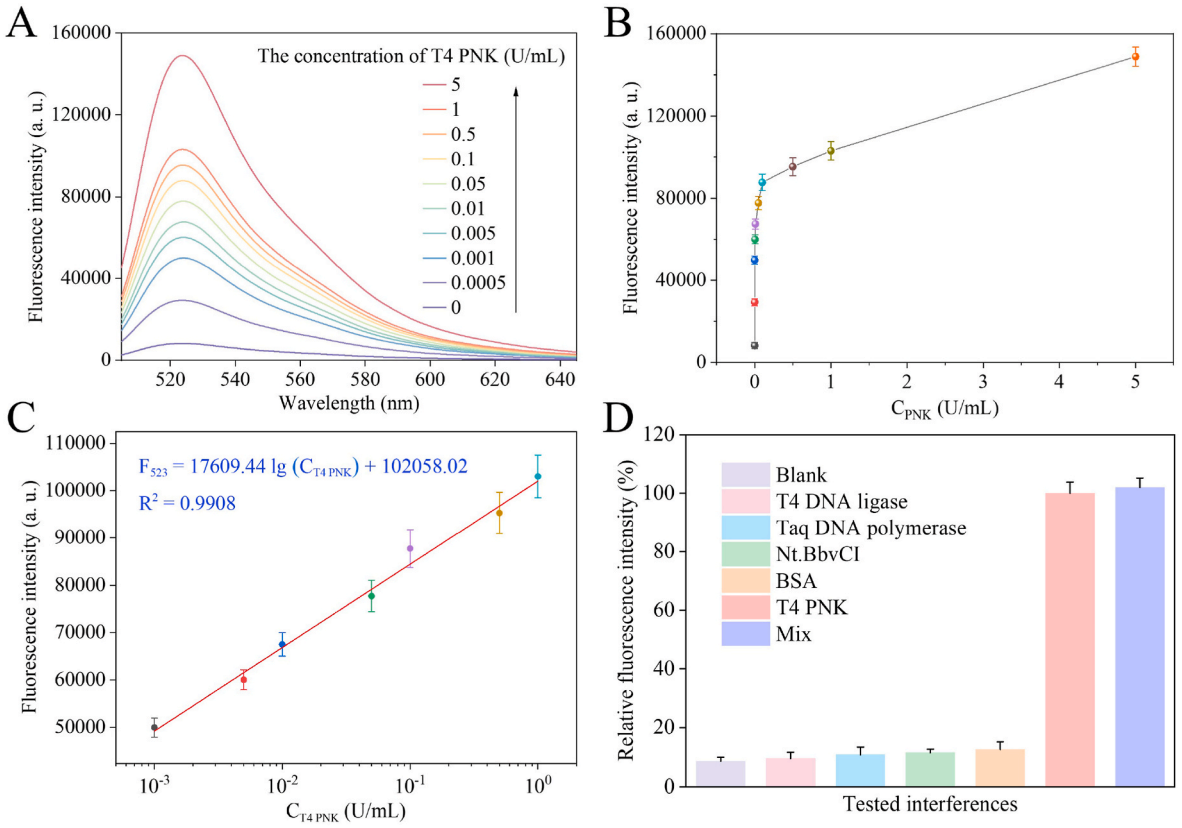


Fig. 3. Quantitative performance and specificity of PHFs-based strategy. (A) Fluorescence spectra at varying T4 PNK concentrations (0–5 U/mL). (B) Peak fluorescent intensity at 523 nm depends on T4 PNK concentration from 0 to 5 U/mL. (C) Linear correlation between peak fluorescent intensity and the logarithm of target concentration from 0.001 to 1 U/mL. (D) Incubation of target and non-targets (T4 DNA ligase, Taq DNA polymerase, Nt. BbvCI, and BSA) at the same concentration with the sensing system to drive the operation of PHFs-based two-stage acceleration strategy for fluorescence emission. Error bars are obtained from at least three repetitive tests. Experimental conditions: [PHFs] = 0.50 μg/mL, [SPs] = 40 nM, [T4 PNK] = 0.05 U/mL, [TdT] = 25 U/mL, [dATPs] = 1 mM, [Cas12a] = 20 nM, [crRNA] = 6 nM, [ssDNA-RM] = 100 nM, [T4 DNA ligase] = 25 U/mL, [Taq DNA polymerase] = [Nt. BbvCI] = 50 U/mL, and [BSA] = 5 mg/mL. The enzymatic reaction time was 20 min, while the reaction time for the CRISPR/Cas12a system was 10 min.

3.4. Quantification performance, specificity, stability, and reproducibility study

The PHF-based two-stage acceleration strategy accurately identifies and quantifies PNK and has a significant potential for early disease diagnosis and therapeutic response monitoring. To assess the detection performance of this strategy for T4 PNK signaling, we conducted quantitative measurements of T4 PNK at concentrations ranging from 0 to 5 U/mL under the same optimized experimental conditions (Fig. S3). As depicted in Fig. 3A, the fluorescence response intensity gradually increased with increasing T4 PNK concentration owing to its increased participation and dephosphorylation performance. The corresponding target-dependent peak fluorescence intensities are shown in Fig. 3B. To accurately show the relationship between the peak fluorescence response and target concentration, we fitted the peak fluorescence value at 523 nm (F_{523}) against the T4 PNK concentration ($C_{T4\ PNK}$) (Fig. 3C). The regression curve was obtained as $F_{523} = 17609.44\ \lg(C_{T4\ PNK}) + 102058.02$ ($R^2 = 0.9908$) when the T4 PNK concentration ranged from 0.001 to 1 U/mL. Based on a 3σ rule, the limit of detection (LOD) was calculated to be approximately 1.82×10^{-4} U/mL [36–38]. Table S2 compares our assay performance with previously reported methods for PNK detection, highlighting methodological advancements in the assay LOD and linear response range.

To demonstrate the specificity of our system for PNK detection, we introduced various competing enzymes and proteins, such as T4 DNA ligase, Taq DNA polymerase, Nt.BbvCI, and BSA, against the target T4 PNK to trigger the operation of this strategy. A blank sample that did not contain any target analyte was used as the control. As shown in Fig. 3D, the signal response triggered by T4 PNK (F_t-F_0) was defined as 100 %. The relative responses caused by other target analytes were calculated using the formula $[(F–F_0)/(F_t-F_0)]$. F_t, F, and F_0 represent the peak fluorescence values of T4 PNK, other non-targets, and blank samples, respectively. The signal differences between the target and non-targets confirmed the specificity of our study. To ensure the practical applicability of PHF, investigations were conducted on its stability. Analysis revealed that the PHF exhibits exceptional storage, reliable batch, and biological stability (Fig. S4). A series of recovery tests were conducted to validate the repeatability of the experimental results (Table S3). The recovery rates ranged from 94.72 % to 104.11 %, which were slightly below 100 %, demonstrating the practicability of our assay. In addition, all relative standard deviations (RSDs) were within 2.0 %, further confirming the reproducibility of the proposed method.

3.5. Inhibition assay for PNK and detection of cellular PNK activity

Screening for effective PNK inhibitors is crucial for drug development, because abnormal PNK expression can cause various diseases. To perform the PNK inhibition assay, we pre-treated PNK with model inhibitors $(NH_4)_2SO_4$ and Na_2HPO_4 for 10 min at 37 °C. Subsequently, we performed the same detection process as that used for PNK activity measurements. Fig. 4A and B demonstrate a gradual decrease in the fluorescence signal as the concentration of the inhibitor increased. The half-maximal inhibitory concentration (IC_{50}) of $(NH_4)_2SO_4$ on PNK was 9.88 mM, whereas the IC_{50} of Na_2HPO_4 was 13.16 mM, which is comparable to previously reported IC_{50} values [39,40]. These findings indicated that our strategy is promising for PNK inhibitor screening and

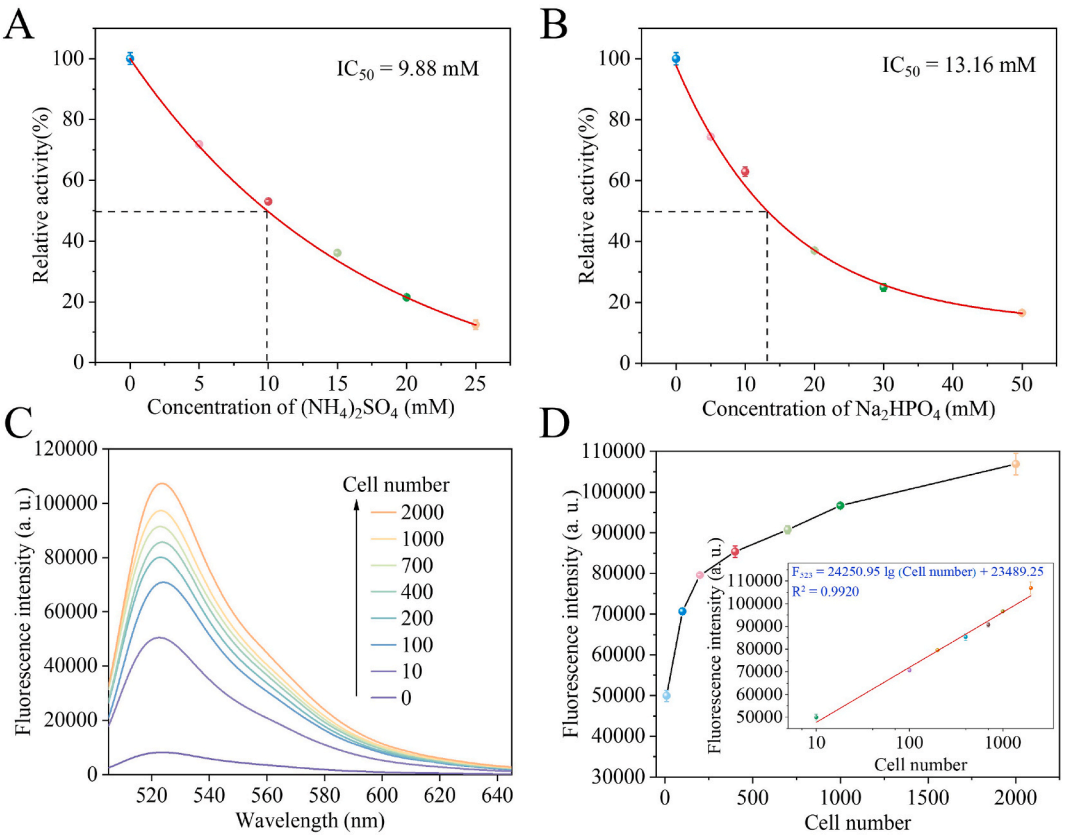


Fig. 4. Inhibition assay and cellular T4 PNK detection. Change of the relative activity of T4 PNK with different concentrations of (A) $(NH_4)_2SO_4$ and (B) NaH_2PO_4. (C) Fluorescence spectra indicative of PNK activity were recorded from Hela cell extracts with varying cell numbers. (D) The changes in fluorescence intensity values reflect PNK activity in Hela cell extracts as cell numbers increase (0−2000). Insert showed a linear relationship between the fluorescence intensity value and the number of cells (10−2000). Error bars are obtained from at least three repetitive tests. Experimental conditions: [PHFs] = 0.50 μg/mL, [SPs] = 40 nM, [TdT] = 25 U/mL, [dATPs] = 1 mM, [Cas12a] = 20 nM, [crRNA] = 20 nM, and [ssDNA-RM] = 100 nM. The enzymatic reaction time was 20 min, while the reaction time for the CRISPR/Cas12a system was 10 min.

drug development. To assess the efficacy of the two-stage acceleration strategy based on PHF for detecting PNK in actual samples, we used HeLa cells as a cellular model to determine the activity of PNK in the cell extracts. Fig. 4C illustrates the fluorescence spectra obtained from our detection system, which were recorded following the analysis of extracts derived from varying cell quantities. As shown in Fig. 4D, the fluorescence signal value of the sensing system increased numerically as the number of cells grew from 0 to 2000. Furthermore, the fluorescence intensity values exhibited a linear correlation with the number of Hela cells, ranging from 10 to 2000, as shown in the inset of Fig. 4D. The regression curve, derived from fitting the peak fluorescence value at a wavelength of 523 nm against the cell number, is expressed as $F_{523} = 24250.95$ lg (cell number) + 23489.25, with an R^2 value of 0.9920. These results validated our strategy's promising potential for practical applications.

4. Conclusions

In summary, we proposed a two-stage accelerated strategy that utilizes PHFs to enhance the performance of TCS for selective, sensitive, and efficient detection of PNK activity. During the first acceleration stage, PHFs effectively enhance the local concentration of phosphorylated 3′ termini of SPs, thereby facilitating collision efficiency between the 3′ termini, PNK, and TdT, ultimately leading to an increased rate of enzymatic reactions. During the second phase of acceleration, PHFs served as the central component for attaching numerous poly-A tails, thereby facilitating the binding of a large quantity of crRNA/Cas12a. This process significantly enhanced the local concentration of the Cas12a protein, improving the efficiency of ssDNA-RM cleavage. PHFs confine the reactants within a confined space, thereby promoting frequent molecular collisions and accelerating multiple enzymatic reactions. The developed sensing strategy enabled the detection of PNK activity in a linear range of 0.001–1 U/mL, with a detection limit of 1.82×10^{-4} U/mL. This strategy has been successfully applied to detect PNK activity in cell extracts and screen PNK inhibitors. Future studies will focus on clinical sample analysis to further validate the diagnostic potential of this strategy. Overall, current research on the development of PHF-based analytical tools capable of detecting biomarkers is expected to offer new and highly promising opportunities for disease diagnosis.

CRediT authorship contribution statement

Qi Wang: Writing – original draft, Validation, Formal analysis. **Xiumei Chen:** Software, Investigation. **Yang Li:** Validation, Formal analysis. **Shuo Yang:** Investigation, Formal analysis. **Suhua Fan:** Formal analysis. **Juan Xia:** Validation, Conceptualization. **Hai Wu:** Writing – review & editing, Supervision, Funding acquisition.

Declaration of competing interest

The authors declare that they have no known competing financial interests or personal relationships that could have appeared to influence the work reported in this paper.

Acknowledgements

This work was financially supported by the Natural Science Foundation of Higher Education Institutions in Anhui Province (grant nos. 2022AH051335, 2022AH040201, and KJ2021ZD0074), the Fuyang Normal University science research project (grants no. 2024KYQD0037), the Master Studio of Graduate Students (grants no. 2022msgzs040), the Scientific Research and Innovation Team of Fuyang Normal University (grants no. kytd202001), the Open Subject of the Provincial Research Platform in Fuyang Normal University (grants no. FSKFKT018D), the Project of Graduate Academic Innovation (grants no. FNU2023xscx001), the Biological and Medical Sciences of Applied Summit Nurturing Disciplines in Anhui Province (Anhui Education Secretary Department, 202313), the Innovative Research Team in University of Anhui Province (2022AH010079), and the National Innovation Training Program for College Students (Grants No. S202410371095).

Appendix A. Supplementary data

Supplementary data to this article can be found online at https://doi.org/10.1016/j.talanta.2025.127981.

Data availability

The authors are unable or have chosen not to specify which data has been used.

References

[1] H. Chen, Z. Wang, X. Chen, K. Lou, A. Sheng, T. Chen, G. Chen, J. Zhang, New method for detection of T4 polynucleotide kinase phosphatase activity through isothermal EXPonential amplification reaction, Analyst 144 (6) (2019) 1955–1959.
[2] T. Jin, J. Zhang, Y. Zhao, X. Huang, C. Tan, S. Sun, Y. Tan, Magnetic bead-gold nanoparticle hybrids probe based on optically countable gold nanoparticles with dark-field microscope for T4 polynucleotide kinase activity assay, Biosens. Bioelectron. 150 (2020) 111936.
[3] A. Chatterjee, S. Saha, A. Chakraborty, A. Silva-Fernandes, S.M. Mandal, A. Neves-Carvalho, Y. Liu, R.K. Pandita, M.L. Hegde, P.M. Hegde, The role of the mammalian DNA end-processing enzyme polynucleotide kinase 3'-phosphatase in spinocerebellar ataxia type 3 pathogenesis, PLoS Genet. 11 (1) (2015) e1004749.
[4] S.M. Yannone, S. Roy, D.W. Chan, M.B. Murphy, S. Huang, J. Campisi, D.J. Chen, Werner syndrome protein is regulated and phosphorylated by DNA-dependent protein kinase, J. Biol. Chem. 276 (41) (2001) 38242–38248.
[5] L.C. Dumitrache, P.J. McKinnon, Polynucleotide kinase-phosphatase (PNKP) mutations and neurologic disease, Mech. Ageing Dev. 161 (2017) 121–129.
[6] Y. Wang, Y. Chen, Y. Wan, C. Hong, J. Shang, F. Li, X. Liu, F. Wang, An autocatalytic DNA circuit based on hybridization chain assembly for intracellular imaging of polynucleotide kinase, ACS Appl. Mater. Interfaces 14 (28) (2022) 31727–31736.
[7] Y. Zhang, R. Li, S. Yu, J. Shang, Y. He, Y. Wang, X. Liu, F. Wang, Sensitive autocatalytic hybridization circuit for reliable in situ intracellular polynucleotide kinase imaging, Anal. Chem. 94 (40) (2022) 13951–13957.
[8] W. Tang, J. Liu, B. Ding, Nucleic acid nanostructure for delivery of CRISPR/Cas9-based gene editing system, Interdis. Med. 1 (1) (2023) e20220014.
[9] W. Li, W. Liu, X. Yang, W.-B. Liang, R. Yuan, Y. Zhuo, Universal signal switch based on a mesostructured silica xerogel-confined ECL polymer for epigenetic quantification, Anal. Chem. 96 (4) (2024) 1651–1658.
[10] J. Zheng, X. Wang, H. Qin, Y. Hou, Q. Yang, X. Zhang, X. Hun, Target-navigated CBT–cys "stapling" coupled with CRISPR/Cas12a amplification for the photoelectrochemical nucleic acid assay, Anal. Chem. 96 (45) (2024) 18011–18019.
[11] X. Wang, H. Qin, Y. Sun, X. Han, W. Li, M. Zhang, Y. Hou, X. Hun, CRISPR/Cas12a coupled with In_2O_3/multiwalled carbon nanotube/PTCDA-EDA-DAP modified electrode self-powered photoelectrochemical assay for EBV-DNA, Sensor. Actuat. B-Chem. 418 (2024) 136274.
[12] Y. Gao, Y.S. Ang, L.-Y.L. Yung, One-pot detection of proteins using a two-way extension-based assay with Cas12a, ACS Sens. 9 (8) (2024) 3928–3937.
[13] J. Xu, T. Zhou, D. Xue, Z. Sui, H. Yang, X. Yuan, Q. Wang, Integrating recombinase polymerase amplification with CRISPR/Cas9-initiated nicking-rolling circle amplification in Staphylococcus aureus assay, Chem. Commun. 60 (40) (2024) 5314–5317.
[14] J. Zhao, Z. Tan, L. Wang, C. Lei, Z. Nie, A ligation-driven CRISPR–Cas biosensing platform for non-nucleic acid target detections, Chem. Commun. 57 (57) (2021) 7051–7054.
[15] X. Wang, D. Zheng, C. Wang, D. Xue, Q. Wang, J. Xia, Harnessing intermolecular G-quadruplex-based spatial confinement effect for accelerated activation of CRISPR/Cas12a empowers ultra-sensitive detection of PML/RARA fusion genes, Anal. Chim. Acta 1287 (2024) 342108.
[16] H. Li, Y. Wang, Y. Wan, M. Li, J. Xu, Q. Wang, D. Wu, Stimuli-responsive incremental DNA machine auto-catalyzed CRISPR-Cas12a feedback amplification permits ultrasensitive molecular diagnosis of esophageal cancer-related microRNA, Talanta 271 (2024) 125675.
[17] Q. Wang, J. Xia, C. Yang, X. Chen, B. Chen, Y. Li, H. Huang, B. Lin, L. Guo, J. Xu, Cross-priming-linked hierarchical isothermal amplification programming progressive activating clustered regularly interspaced short palindromic repeats/Cas12a in miRNA signaling, Anal. Chem. 96 (35) (2024) 14205–14214.
[18] Q. Wang, B. Chen, D. Zheng, J. Xia, L. Wu, J. Xu, Intramolecular accelerated assembly of molecular beacons: a DNA nanoarchitecture-based spatial confinement strategy toward terminal deoxynucleotidyl transferase biosensing, Anal. Chem. 95 (36) (2023) 13708–13715.
[19] X. Zhang, C. Zheng, L. Ding, Y. Wu, H. Xu, Y. Sun, Y. Zeng, X. Liu, J. Liu, CRISPR-Cas12a coupled with terminal deoxynucleotidyl transferase mediated isothermal

amplification for sensitive detection of polynucleotide kinase activity, Sensor. Actuat. B-Chem. 330 (2021) 129317.
[20] Y.-C. Du, S.-Y. Wang, Y.-X. Wang, J.-Y. Ma, D.-X. Wang, A.-N. Tang, D.-M. Kong, Terminal deoxynucleotidyl transferase combined CRISPR-Cas12a amplification strategy for ultrasensitive detection of uracil-DNA glycosylase with zero background, Biosens. Bioelectron. 171 (2021) 112734.
[21] L.-P. Xu, Y. Chen, G. Yang, W. Shi, B. Dai, G. Li, Y. Cao, Y. Wen, X. Zhang, S. Wang, Ultratrace DNA detection based on the condensing-enrichment effect of superwettable microchips, Adv. Mater. 27 (43) (2015) 6878–6884.
[22] K. Ren, Y. Xu, Y. Liu, M. Yang, H. Ju, A responsive "nano string light" for highly efficient mRNA imaging in living cells via accelerated DNA cascade reaction, ACS Nano 12 (1) (2018) 263–271.
[23] L. Liu, Q. Rong, G. Ke, M. Zhang, J. Li, Y. Li, Y. Liu, M. Chen, X.-B. Zhang, Efficient and reliable microRNA imaging in living cells via a FRET-based localized hairpin-DNA cascade amplifier, Anal. Chem. 91 (5) (2019) 3675–3680.
[24] X. Hun, Y. Meng, Electron acceptors co-regulated self-powered photoelectrochemical strategy and its application for circulating tumor nucleic acid detection coupled with recombinase polymerase amplification, Anal. Chem. 92 (17) (2020) 11771–11778.
[25] X. Ding, J. Ma, T. Fan, R. Issa, Y. Li, D. Weng, D. Zhang, Y. Chen, Inorganic nanoparticles-based strategies for the microbial detection in infectious diseases, Interdis. Med. 2 (2) (2024) e20230045.
[26] Y. Zhu, W. Li, F. Lan, S. Chen, X. Chen, X. Zhang, X. Yan, Y. Zhang, DNA nanotechnology in tumor liquid biopsy: enrichment and determination of circulating biomarkers, Interdis. Med. 2 (1) (2024) e12080.
[27] X. Wang, J. Zheng, H. Qin, Y. Zong, X. Hun, Self-powered organic semiconductor photoelectrochemical strategy via CBT-Cys reaction for HSV-1 DNA detection, Microchem. J. 209 (2025) 112762.
[28] H. Zhang, L.-Y. Guo, J. Jiao, X. Xin, D. Sun, S. Yuan, Ionic self-assembly of polyoxometalate–dopamine hybrid nanoflowers with excellent catalytic activity for dyes, ACS Sustain. Chem. Eng. 5 (2) (2017) 1358–1367.
[29] S.S. Nadar, S.D. Gawas, V.K. Rathod, Self-assembled organic-inorganic hybrid glucoamylase nanoflowers with enhanced activity and stability, Int. J. Biol. Macromol. 92 (2016) 660–669.
[30] J. Cui, S. Jia, Organic–inorganic hybrid nanoflowers: a novel host platform for immobilizing biomolecules, Coord. Chem. Rev. 352 (2017) 249–263.
[31] Y. Wang, G. Zhao, H. Chi, S. Yang, Q. Niu, D. Wu, W. Cao, T. Li, H. Ma, Q. Wei, Self-luminescent lanthanide metal–organic frameworks as signal probes in electrochemiluminescence immunoassay, J. Am. Chem. Soc. 143 (1) (2020) 504–512.
[32] X. Zhang, J. Xu, X. Xing, L. Yao, H. Shang, W. Chen, Framework nucleic acid-wrapped protein-inorganic hybrid nanoflowers with three-stage amplified fluorescence polarization for terminal deoxynucleotidyl transferase activity biosensing, Biosens. Bioelectron. 193 (2021) 113564.
[33] Z. Zhao, Z. Xie, S. Chen, M. Chen, X. Wang, G. Yi, A novel biosensor based on tetrahedral DNA nanostructure and terminal deoxynucleotidyl transferase-assisted amplification strategy for fluorescence analysis of uracil-DNA glycosylase activity, Anal. Chim. Acta 1271 (2023) 341432.
[34] W. Tian, G. Wang, X. Liu, W. Ren, C. Liu, Z. Li, A terminal extension-actuated isothermal exponential amplification strategy toward the ultrasensitive and versatile detection of enzyme activity in a single cell, Talanta 211 (2020) 120704.
[35] J.S. Chen, E. Ma, L.B. Harrington, M. Da Costa, X. Tian, J.M. Palefsky, J.A. Doudna, CRISPR-Cas12a target binding unleashes indiscriminate single-stranded DNase activity, Science 360 (6387) (2018) 436–439.
[36] Q. Wang, T. Zhou, D. Xue, H. Yang, Z. Sui, X. Yuan, J. Xu, An allosteric palindromic hairpin probe based dual-mode interactive strand displacement amplification enables robust miRNA biosensing, Chem. Commun. 60 (21) (2024) 2910–2913.
[37] J. Xia, Z. Liu, S. Gao, Q. Wang, J. Xu, H. Wu, Intermolecular and intramolecular priming Co-directed synergistic multi-strand displacement amplification empowers ultrasensitive determination of microRNAs, Anal. Chem. 94 (46) (2022) 16132–16141.
[38] Q. Wang, W. Li, J. Xia, H. Wu, L. Wu, J. Xu, Stepwise tuning of a molecular beacon coupled Y probe regulates ternary DNA nanomachine-based microRNA determination, Sensor. Actuat. B-Chem. 363 (2022) 131858.
[39] X.-Y. Li, Y.-X. Cui, Y.-C. Du, A.-N. Tang, D.-M. Kong, Isothermal cross-boosting extension–nicking reaction mediated exponential signal amplification for ultrasensitive detection of polynucleotide kinase, Analyst 145 (10) (2020) 3742–3748.
[40] Y.-P. Zhang, Y.-X. Cui, X.-Y. Li, Y.-C. Du, A.-N. Tang, D.-M. Kong, A modified exponential amplification reaction (EXPAR) with an improved signal-to-noise ratio for ultrasensitive detection of polynucleotide kinase, Chem. Commun. 55 (53) (2019) 7611–7614.